
KITP 2004

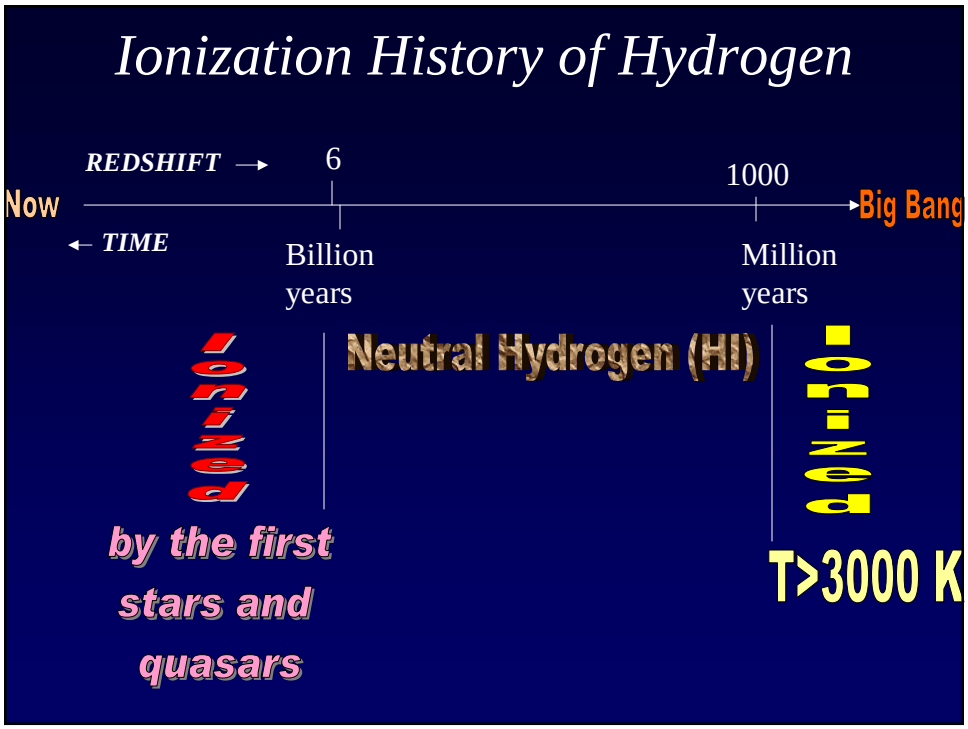
Ionization History of Hydrogen
REDSHIFT
6
1000
Now
Big Bang
TIME
Billion years
Million years
ionized
Neutral Hydrogen (HI)
ionized
by the first stars and quasars
T>3000 K

Emergence of the First Star Clusters

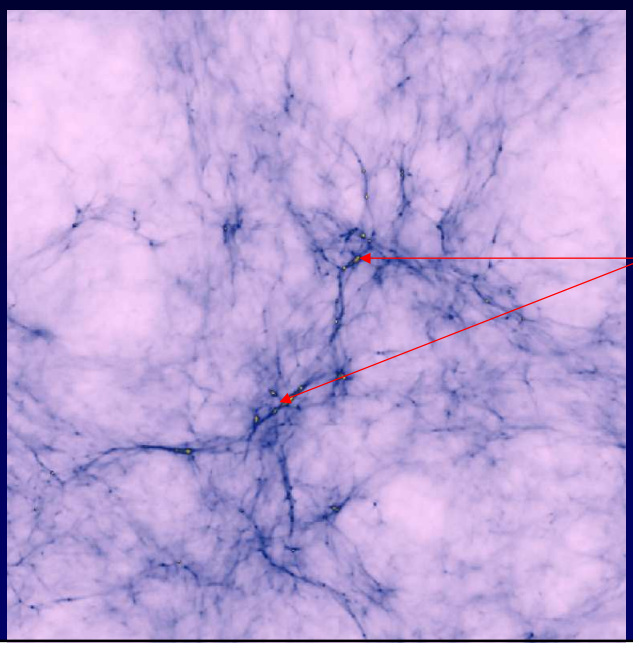

Yoshida et al. 2003

Hydrogen

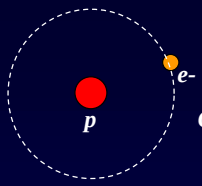

Ground level

excitation rate= (atomic collisions)+(radiative coupling to CMB)

Couple T_s *to* T_k *Couples* T_s *to* $T_í$

spin

21cm = (1:4GHz) ^{1}

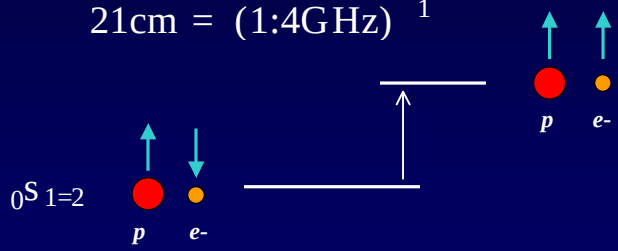

Spin Temperature $\frac{n_1}{n_0} = \frac{g_1}{g_0} \exp f\,à\ \frac{0:068K}{T_s} g$ $(g_1=g_0) = 3$

Predicted by Van de Hulst in 1944; Observed by Ewen &Purcell in 1951 at Harvard

21 cm Absorption by Hydrogen Prior to Structure Formation

$$T_b = \text{ü}\ \frac{T_s \text{à}\ T_{\text{í}}}{1+z} \qquad T_b = 28\text{mK}\ \frac{1+z}{10}^{1=2}\ \frac{T_s \text{à}\ T_{\text{í}}}{T_s}$$

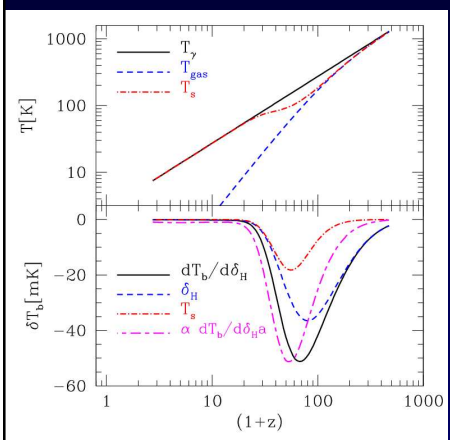

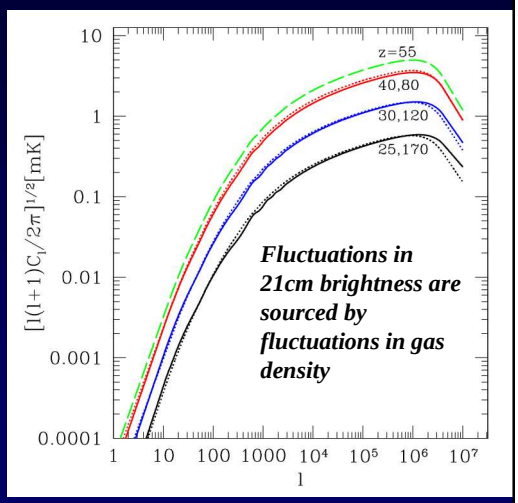

Loeb & Zaldarriaga, Phys. Rev. Lett., 2004; astro-ph/0312134

Observed wavelength=21cm (1+z) → 3D tomography (slicing the universe in redshift)

Largest Data Set on the Sky

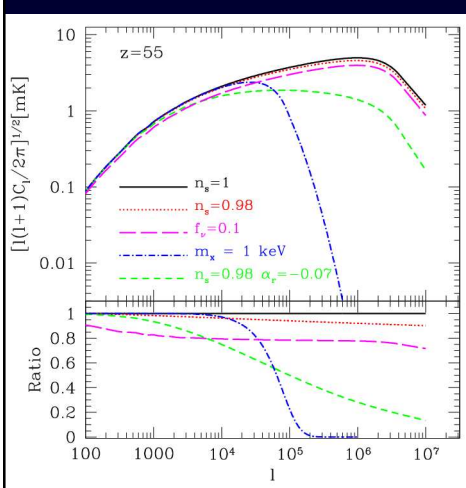

Number of independent patches:

$$\text{ø}\ 10^{16}\ \frac{l_{max}}{10^6}^{3}\ \frac{\text{É} \div}{\div}$$

while Silk damping limits the primary CMB anisotropies to only ø 10^7

Noise due to foreground sky brightness:

$$N_\nu \sim 0.4\ \text{mK} \left(\frac{I_\nu}{5\times10^5\ \text{Jy sr}^{-1}}\right)\left(\frac{l_{min}}{35}\right)\left(\frac{5000}{l_{max}}\right)\left(\frac{0.016}{f_{cover}}\right) \times \left(\frac{1\ \text{year}}{t_0}\right)^{1/2}\left(\frac{\Delta\nu}{\nu}\right)^{-1/2}\left(\frac{50\ \text{MHz}}{\nu}\right)^{5/2},$$

Loeb & Zaldarriaga, Phys. Rev. Lett., 2004; astro-ph/0312134

Line-of-Sight Anisotropy of 21cm Flux Fluctuations

$$T_b = \ddot{u}\ \frac{T_s \grave{a}\ T_{\acute{i}}}{1+z}$$

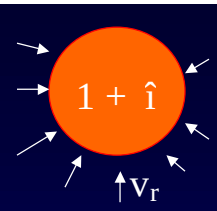

Peculiar velocity changes $\ddot{u} / \frac{n_{HI}}{dv_r = dr} = \ddot{o}(1+\hat{i}) \ \ \emptyset\ H(1 \grave{a}\ \frac{1}{3}\hat{i})$

→ *Power spectrum is not isotropic*

$\frac{dv_r}{dr}$! $\quad \hat{i}_v(\tilde{k}) = \grave{a}\ \cos^2 \grave{o}_k\ \hat{a}\ \hat{i}(\tilde{k})$

$$P_{T_b} = [\cos^2 \grave{o}_k \hat{i}(\tilde{k}) + \hat{i}_{iso}(\tilde{k})]^2$$

$$\hat{i}_{iso} = \grave{\imath}\ \hat{i} + \hat{i}_{x_{HI}} + \hat{i}_T + :::$$

$\cos^4 \grave{o}_k; \cos^2 \grave{o}_k; \cos^0 \grave{o}_k$ ***terms allow separation of powers***

Barkana & Loeb, astro-ph/0409572

Enhancement of 21cm Fluctuations During the Period of Initial Lya Coupling of the spin T to the kinetic T

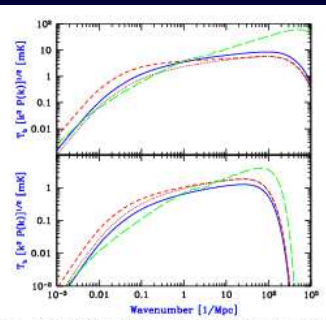

FIG. 1. Observable power spectra during the period of initial Lyα coupling. *Upper panel:* Assumes adiabatic cooling. *Lower panel:* Assumes pre-heating to 500 K by X-ray sources. We show $P_{\mu^4} = P_\delta$ (solid curves), P_{μ^2} (short-dashed curves), and $P_{\mu_n - \delta}$ (long-dashed curves). We also show for comparison $2\beta P_\delta$ (dotted curves).

Wouthuysen-Field Effect

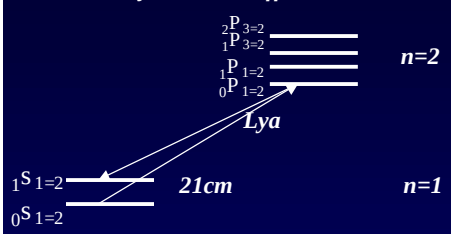

Fluctuations in the distribution of galaxies induce fluctuations in Lya intensity →21cm

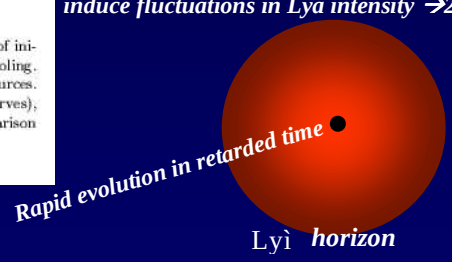

Barkana & Loeb, astro-ph/0410129

Enhancement of 21cm Fluctuations During the Epoch of Initial Lya Coupling

Sourced by fluctuations in Lya intensity from galaxies

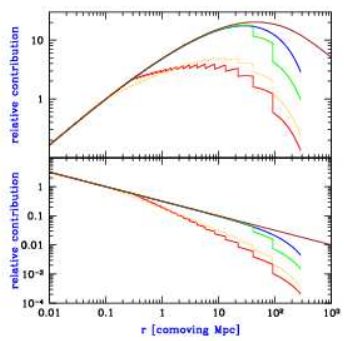

FIG. 1.— Relative contribution per log(r) of shells at various radii r from a gas element at redshift $z = 20$, to the fluctuations in the Lyα flux. We consider the fluctuations sourced by density inhomogeneities (top panel) and by Poisson fluctuations (bottom panel). In each set of solid curves, we show from top to bottom (at large r) the asymptotic case of a non-expanding universe followed by galaxies, where we include stellar radiation emitted up to Lyβ, Lyδ, or full emission (see text). The minimum galaxy mass is set by the atomic cooling threshold in dark matter halos. Inside galaxies, we assumed a fixed star formation efficiency and a Pop III stellar population. Also shown for comparison is the case of full emission with Pop II stars (dotted line). All curves are arbitrarily normalized to unity at $r = 0.1$ Mpc.

Power spectrum of 21cm brightness fluctuations

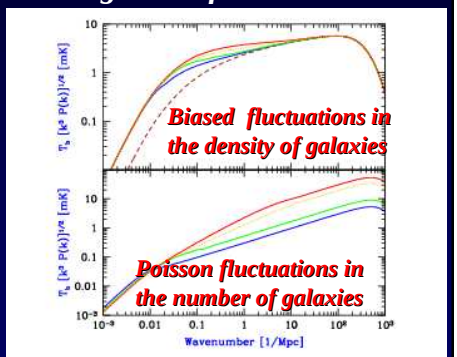

FIG. 2.— Power spectra of 21cm brightness fluctuations. Shown are $P_{\delta T}$ (top panel), which contains the contribution of the density-induced fluctuations in flux, and $P_{\delta m-\delta}$ (bottom panel), which is solely due to the Poisson-induced fluctuations. We assume that galaxies formed via atomic cooling in halos at $z = 20$ with a fixed star formation efficiency in all halos, set to produce the coupling transition at this redshift (so that $x_{tot} = 1$). We also assume that the IGM gas has been cooling adiabatically down to this redshift. In each set of solid curves we include, from bottom to top at $k = 0.1$ Mpc^{-1}, stellar radiation emitted up to Lyβ, Lyδ, or full emission (see text), assuming Pop III stars. Also shown for comparison is the case of full emission with Pop II stars (dotted line). We also show $2\beta P_\delta$ (dashed curve).

Thermal History

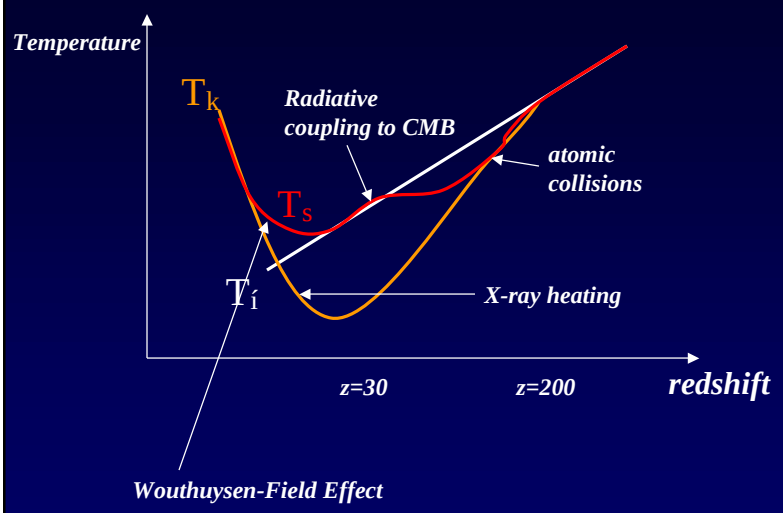

History of 21cm Brightness Fluctuations

- $30 < z < 200$ — **HI appears in absorption against the CMB**

  $T_k < T_{cmb}$ with $T_k < T_s < T_{cmb}$

- $20 < z < 30$

  X-ray heating to $T_k > T_{cmb} = 2$ â $10^{à\ 3}$eV[(1 + z)=10]

  Lya coupling of spin temperature T_s *to kinetic temperature* T_k

  HI appears in emission against the CMB

- $6 < z < 20$

  Reionization: HI gradually disappears

21cm Tomography of Ionized Bubbles During Reionization is like

Slicing Swiss Cheese

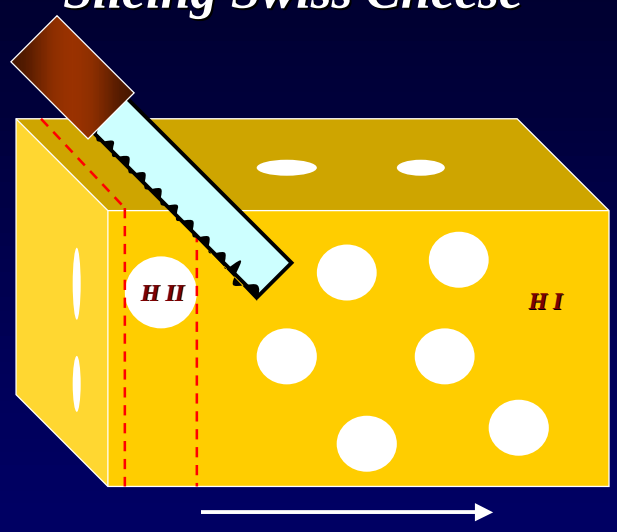

Observed wavelength ⇔ distance

21cm â (1 + z)

Experiments

**MWA (Mileura Wide-Field Array)*

MIT/ATNF/CfA

**LOFAR (Low-frequency Array)*

Netherlands

**PAST (Primeval Structure Telescope)*

China/CITA

**Enhanced VLA*

CfA/NRAO

**SKA (Square Kilometer Array)*

When was the Universe Reionized?

Empirical Hints

First Year Data from WMAP

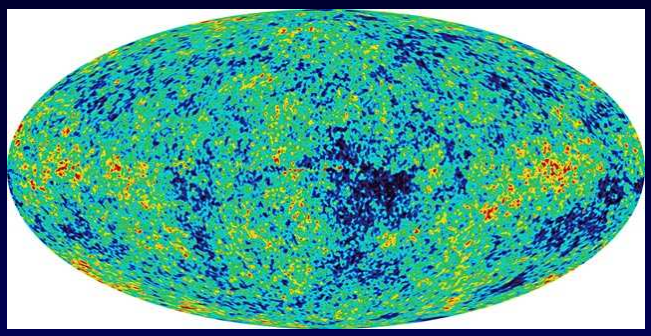

Polarization/temperature correlation implies an electron-scattering optical depth after cosmological recombination at z=1088 of:

= 0:17 0:04

Implying that the universe was reionized at Only 200 million years after the big bang z = 17 5

Kogut et al. 2003

Cosmic Hydrogen was significantly Neutral at z~6.3

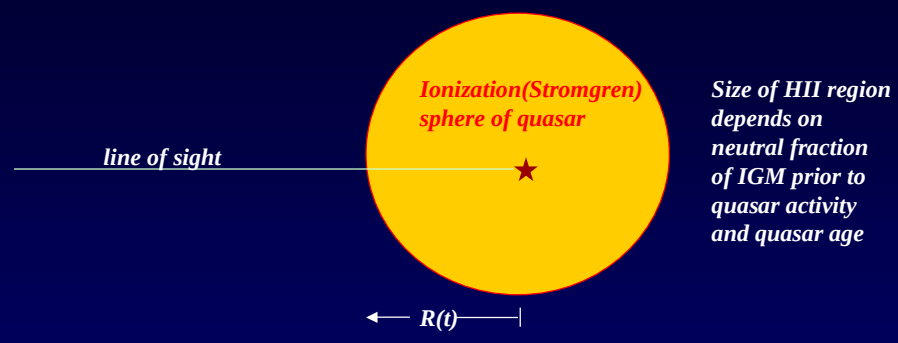

Size of HII region depends on neutral fraction of IGM prior to quasar activity and quasar age

$$\frac{dR}{dt} = c(1+z)\left[\frac{F_\gamma \dot{N}_{\rm ion} - \alpha_{\rm B} C F_{\rm m} x_{\rm HI} \left(\bar{n}_0^{\rm H}\right)^2 (1+z)^3 \left(\frac{4\pi}{3} R^3\right)}{F_\gamma \dot{N}_{\rm ion} + 4\pi R^2 (1+z)\, c F_{\rm m} x_{\rm HI} \bar{n}_0^{\rm H}}\right]$$

Wyithe & Loeb, Nature, 2004; astro-ph/0401188

The Earliest Quasar Detected: z=6.4

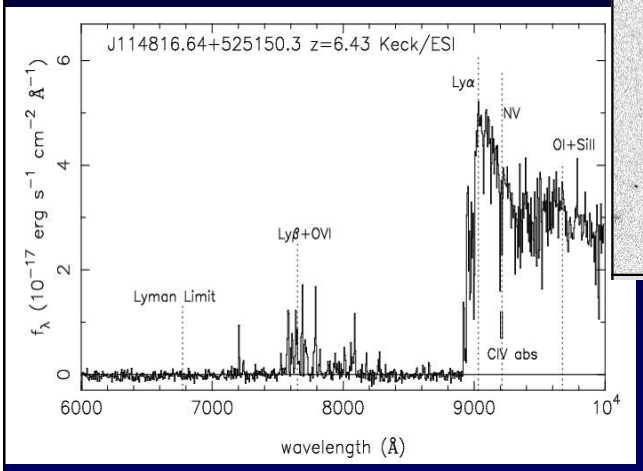

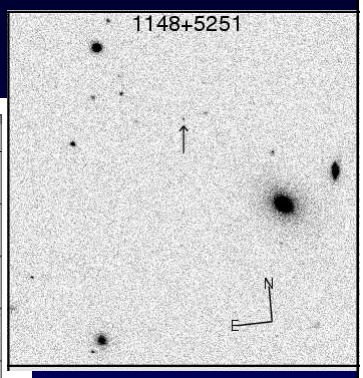

Fan et al. 2002

Likelihood for Neutral Fraction x_{HI} *at z~6.3*

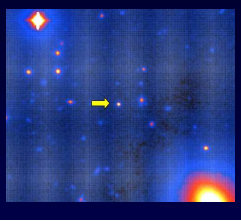

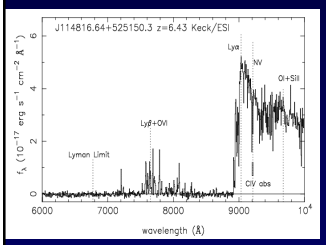

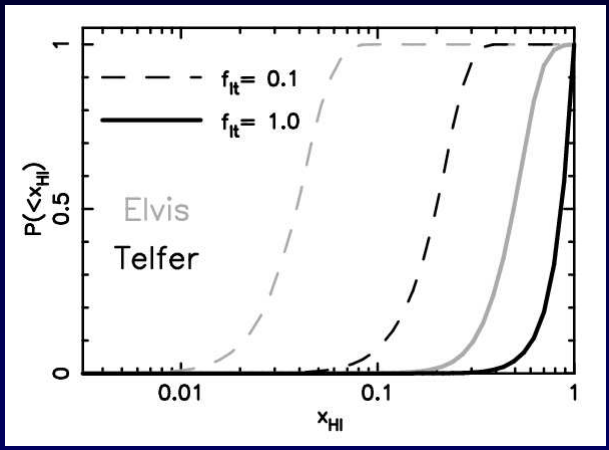

quasar lifetime = 4 â $10^7 f_{lt}$ ï/0:1 years $\frac{(M_1+M_2)^{5=3}}{M_1^{5=3}+M_2^{5=3}}$

Five quasars instead of two: P ! $P^{5=2}$

Imaging the Neutral Fraction in 21cm

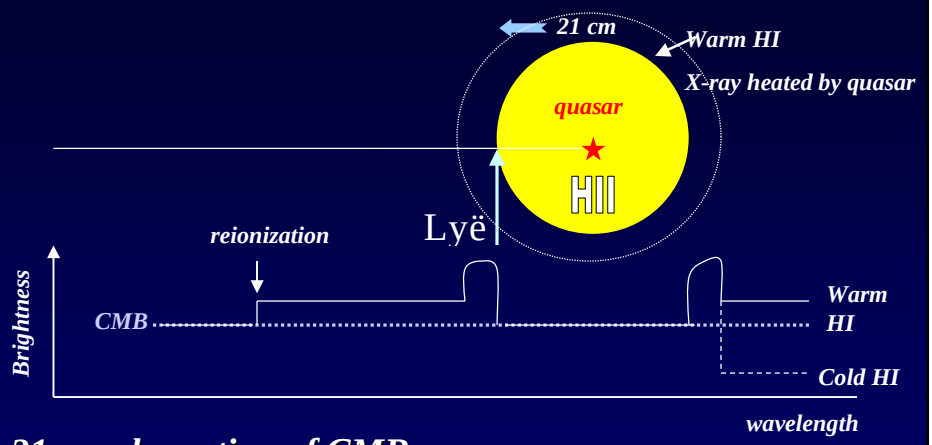

21 cm absorption of CMB **if IGM is cold** ***or***
21 cm emission **due to heating by X-ray background or quasar X-rays (but no Lyman-alpha heating by the quasar)**

~100x relic shells per known quasar

Wyithe and Loeb 2004; astro-ph/0401554

Emission from an X-ray Heated IGM

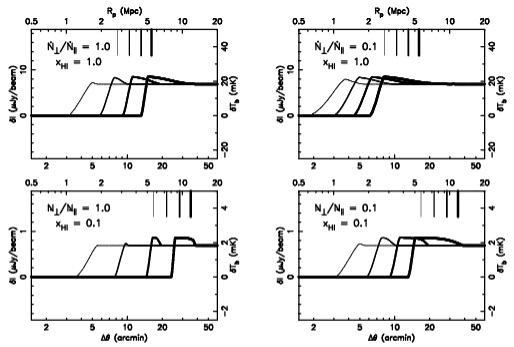

FIG. 4.— Four examples of the evolution of a Strömgren sphere expanding into a warm ($T_{IGM} = 5T_{CMB}$) IGM as seen in redshifted 21cm emission and Lyα absorption, assuming different combinations of $\dot{N}_\perp/\dot{N}_\parallel = 1.0, 0.1$ and $x_{HI} = 1.0, 0.1$. In all cases we assume $R_0 = 0$. The 21cm emission signal is plotted as a function of radius (upper horizontal axes) and apparent angle in arc-minutes (lower axes). The y-axes are labeled by the differential antenna temperature δT_b (right axes) and the flux δI (left axes) given a circular top-hat beam with a diameter of $2'$. In each case, four profiles are shown for observing times corresponding to quasar ages of $t_{age,e} = 0.5, 1, 2, 4 \times 10^7$ yr when the *optical photons* were emitted. Values of R_{Ly} at $t_{age,e} = 0.5, 1, 2, 4 \times 10^7$ yr are shown with tick marks.

Wyithe & Loeb 2004; astro-ph/0401554

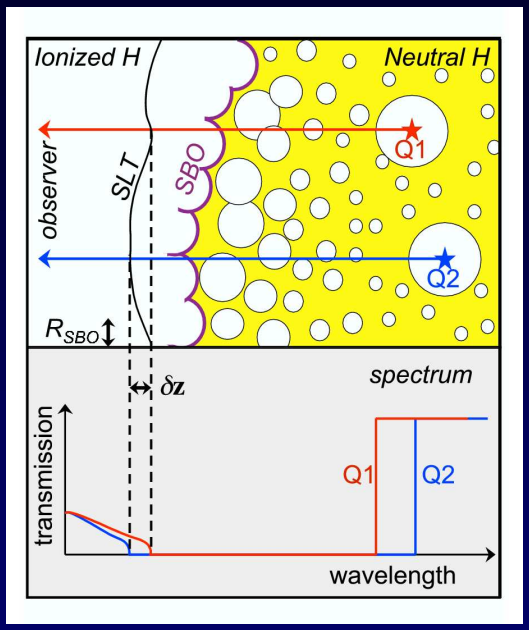

The Characteristic Size of Ionized Bubbles at the End of Reionization

SBO: Surface of Bubble Overlap
SLT: Surface of Lya Transmission

Wyithe & Loeb, Nature, 2004

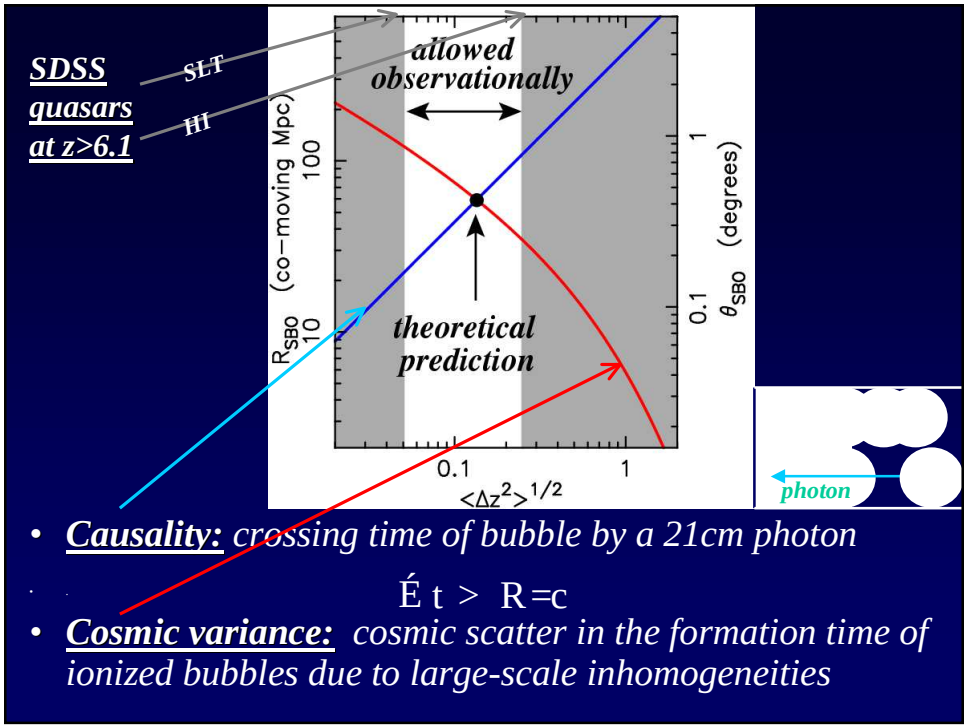
SDSS quasars at z>6.1
SLT
HI
allowed observationally
theoretical prediction
R_{SBO} (co−moving Mpc)
100
10
0.1
1
θ_{SBO} (degrees)
0.1
1
$<\Delta z^2>^{1/2}$
photon
• Causality: crossing time of bubble by a 21cm photon
É t > R=c
• Cosmic variance: cosmic scatter in the formation time of ionized bubbles due to large-scale inhomogeneities

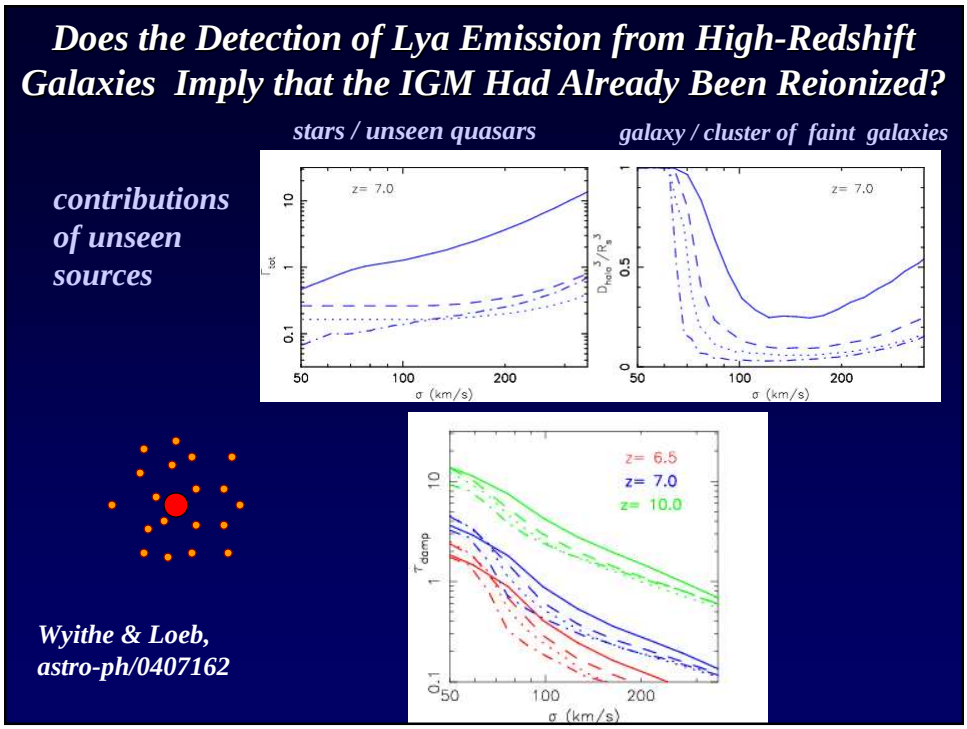
Does the Detection of Lya Emission from High-Redshift Galaxies Imply that the IGM Had Already Been Reionized?
stars / unseen quasars
galaxy / cluster of faint galaxies
contributions of unseen sources
z= 7.0
z= 7.0
σ (km/s)
σ (km/s)
z= 6.5
z= 7.0
z= 10.0
σ (km/s)
Wyithe & Loeb, astro-ph/0407162

A Galaxy at a Redshift 10?

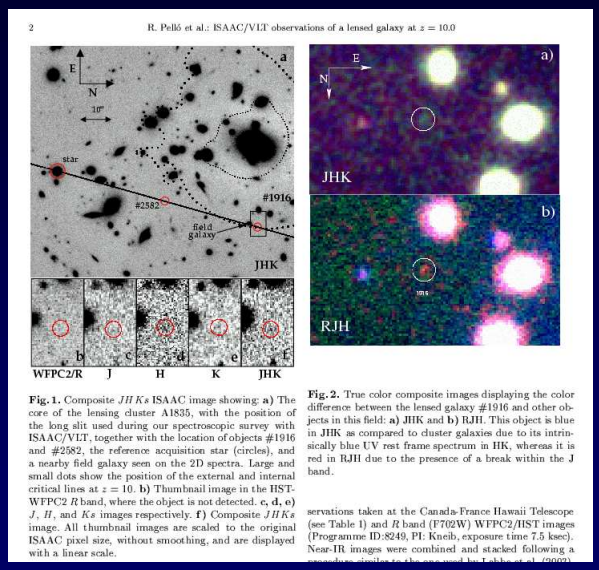

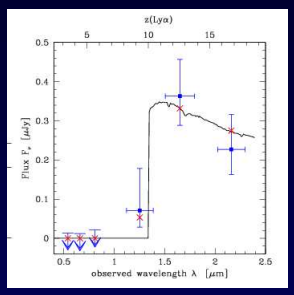

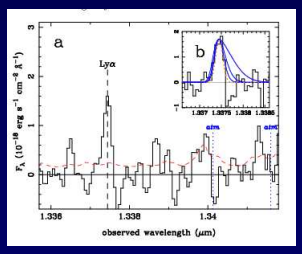

Pello et al., 2004; astro-ph/0403025

But if it were, was the IGM Reionized at z=10?

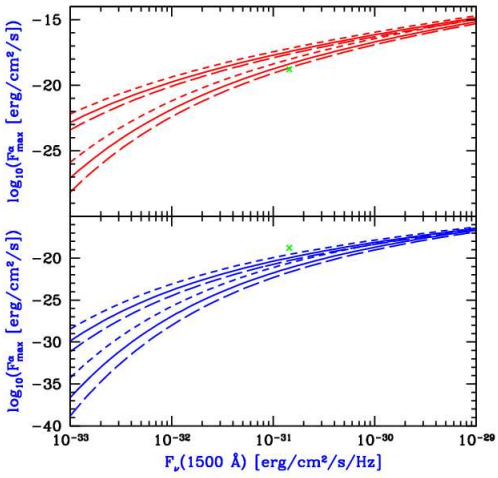

Fig. 1.— Maximum observable flux of the Lyα line versus UV continuum flux (at a rest-frame wavelength of 1500Å) of a galaxy prior to reionization (i.e., assuming that the H II region of the galaxy is surrounded by a neutral IGM). We assume a narrow emission line ($\lesssim 100$ km s^{-1}). We consider a Scalo (1998) IMF (bottom panel) or a Pop III IMF (top panel), at redshifts 7 (short-dashed curves), 10 (solid curves), or 13 (long-dashed curves). In each case, a pair of curves are shown, corresponding to $t_S = 10^8$ yr (higher) or $t_S = 10^7$ yr (lower). Also shown are the observed flux values for the Pello et al. (2004) $z = 10$ galaxy, demagnified by a factor of 25 (denoted by $\times$).

- Neutral fraction <0.4 in the large-scale region around that galaxy, or galaxy harbors metal-free stars that create a sufficiently large HII region in IGM.
- Lya damping wing from outside Stromgren sphere allows Lya line transmission.
- Resonant absorption inside Stromgren sphere may be suppressed by peculiar velocity relative to IGM.

Loeb, Barkana, & Hernquist 2004; astro-ph/0403193

Theoretical Insights

(i) Should we trust numerical simulations or analytic models?

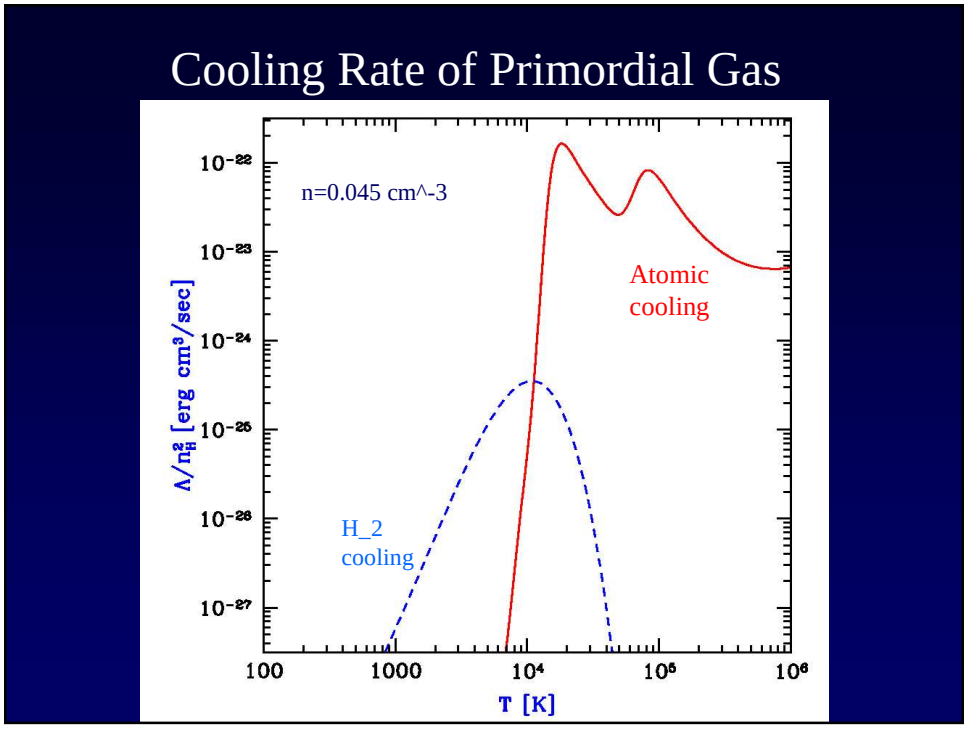
Cooling Rate of Primordial Gas
n=0.045 cm^-3
Atomic cooling
H_2 cooling
Λ/n_H^2 [erg cm^3/sec]
T [K]

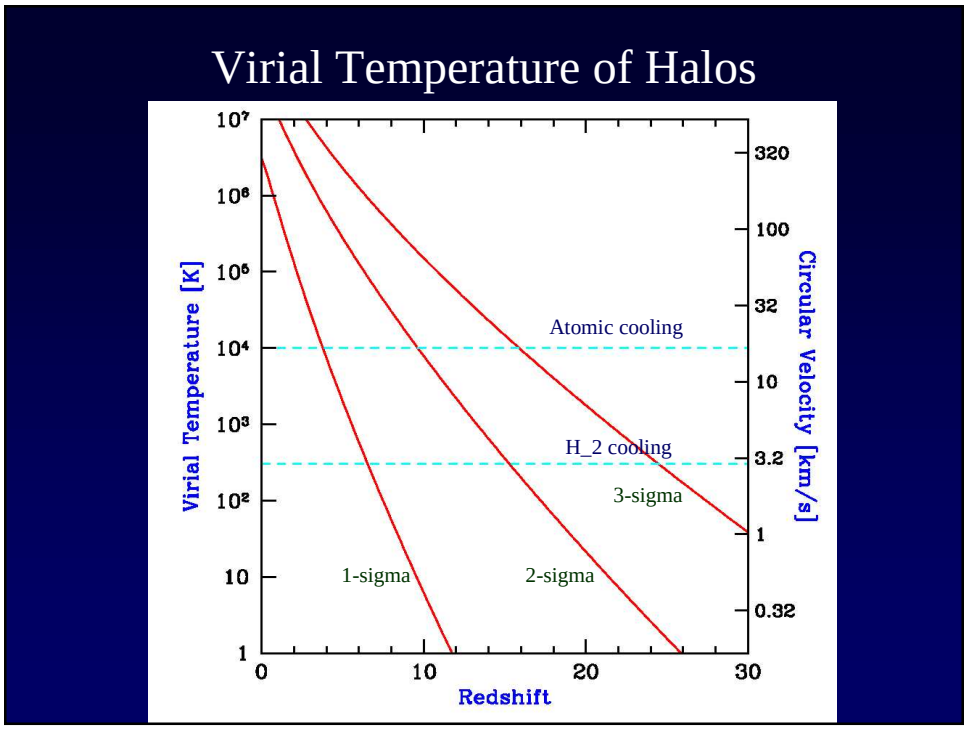
Virial Temperature of Halos
Atomic cooling
H_2 cooling
3-sigma
2-sigma
1-sigma
Virial Temperature [K]
Circular Velocity [km/s]
Redshift

Unusually Large Fluctuations in the Statistics of Galaxy Formation at High Redshifts

Bias in numerical simulations:

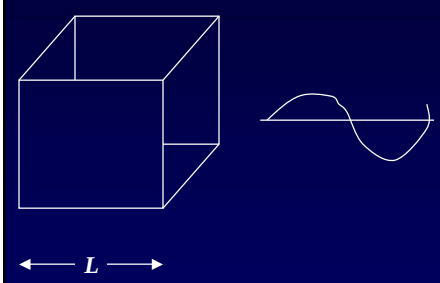

Assumption : $\hat{\imath}_L = 0$

Barkana & Loeb, ApJ, 2003; astro-ph/0310338

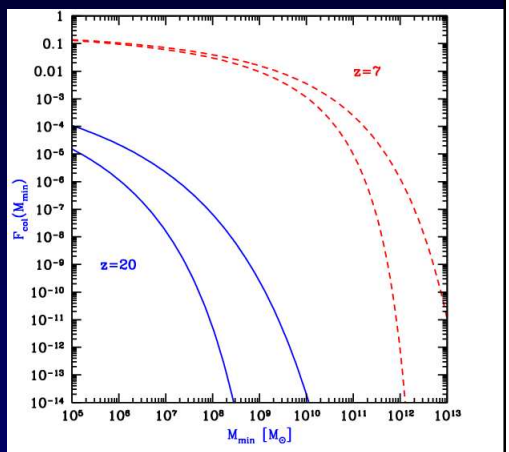

Figure 1: Bias in the halo mass distribution in simulations. We consider the total amount of mass contained in all halos of individual mass $M_{\rm min}$ or greater, expressed as a fraction of the total mass in a given volume. This cumulative fraction $F_{\rm col}(M_{\rm min})$ is shown as a function of the minimum halo mass $M_{\rm min}$. We consider $z = 20$, $l_{\rm box} = 1$ Mpc (solid curves), and $z = 7$, $l_{\rm box} = 6$ Mpc (dashed curves). At each redshift, we compare the true average distribution in the universe (upper curve) to the biased distribution that would be measured in a simulation box with periodic boundary conditions (for which δ_R is artificially set to zero).

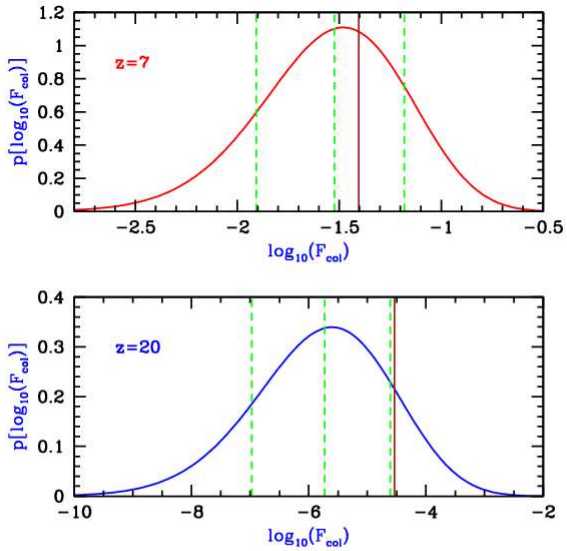

Figure 2: Probability distribution within a small volume of the total mass fraction in galactic halos. The normalized distribution of $\log_{10}$ of this fraction $F_{\rm col}(M_{\rm min})$ is shown for two cases: $z = 20$, $l_{\rm box} = 1$ Mpc, $M_{\rm min} = 7 \times 10^5 M_\odot$ (bottom panel), and $z = 7$, $l_{\rm box} = 6$ Mpc, $M_{\rm min} = 10^8 M_\odot$ (upper panel). In each case, the value in a periodic box ($\delta_R = 0$) is shown along with the value that would be expected given a plus or minus $1-\sigma$ fluctuation in the mean density of the box (dashed vertical lines). Also shown in each case is the mean value of $F_{\rm col}(M_{\rm min})$ averaged over large cosmological volumes (solid vertical line).

(ii) Was Reionization Caused by Metal-Free or Metal-Rich Stars?

Massive Accretion by Pop-III Proto-Stars

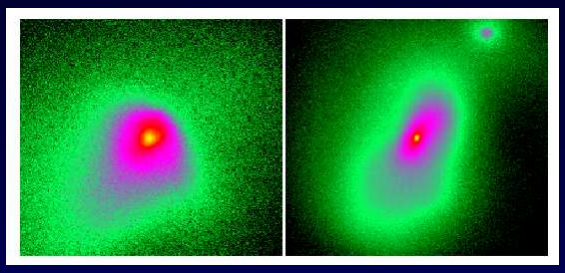

23.5pc *0.5pc*

Resolving accretion flow down to ~0.03 pc

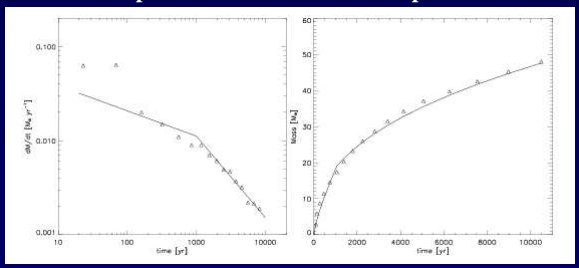

Bromm & Loeb, New Astronomy, 2004; astro-ph/0312456

Number of ionizing photons (>13.6eV) per baryon incorporated into stars:

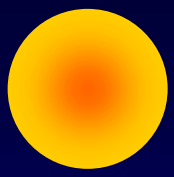

Massive, metal free stars

M > 300M¡	100; 000
M > 100M¡	40; 000

T_{eff} ø 10^5K
L = L_E / M

Gain by up to a factor of ~30!

Salpeter mass function

Metal free	7; 000
Z = 0:01Z¡	3; 500

Bromm, Kudritzki, & Loeb 2001, ApJ, 552, 464

SPH Simulation of a Hypernova Explosion

E_{SN} = 10^{53}ergs; E_{vir} = 10^{51}ergs

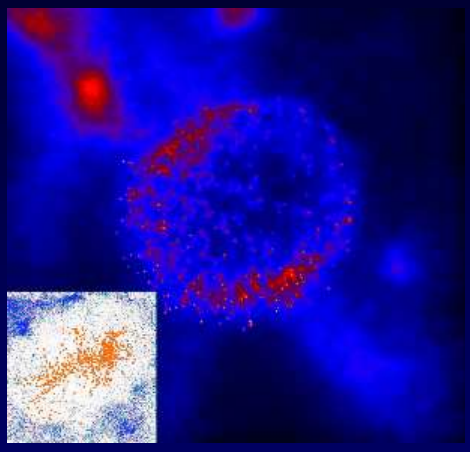

1kpc

Bromm, Yoshida, & Hernquist 2003

Minimum Carbon and Oxygen Abundance Required for the Formation of Low-Mass Stars

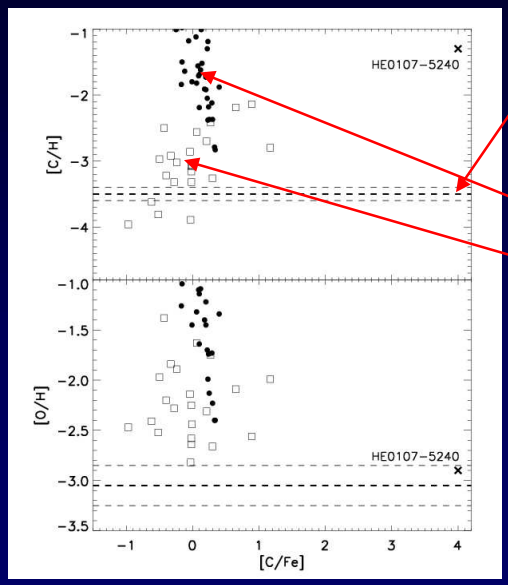

Lines: $t_{cooling} < t_{collapse}$

Cooling rate by C II or O I allows fragmentation in metal-poor gas clumps

Filled points: *halo dwarf stars*

Open squares: *giant stars*

$n \sim 10^4$ cm^{-3}

$T \sim 100 - 200$ K

$M_J \sim 100 M_\odot$

Bromm & Loeb, Nature, 2003; astro-ph/0310622

Reionization Histories of H, He

Free Parameters: *(i) transition redshift, z_{tran}, above which the stellar IMF is dominated by massive, zero-metallicity stars; (ii) the product of the star formation efficiency and the escape fraction of ionizing photons in galaxies, $f_{esc} f_*$.*

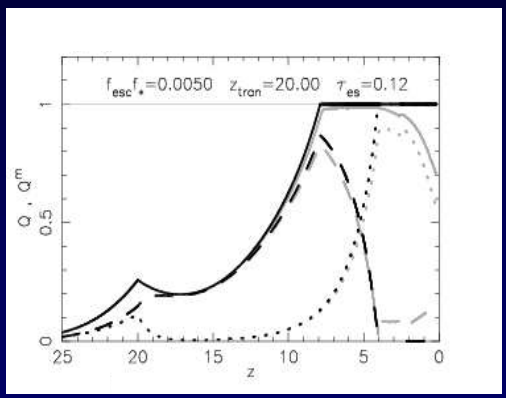

H+

He+

He++

Quasar model fits luminosity function data up to z=6

Wyithe & Loeb 2002

Visibility Function due to Electron Scattering

Scattering probability per conformal time: $g = \dot{\tau}_e$

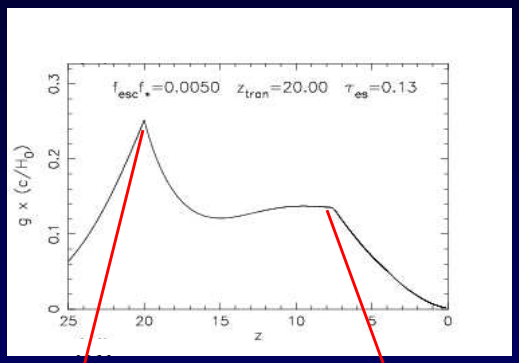

failed overlap *successful overlap*

Wyithe & Loeb 2002

Is double-reionization physically plausible?

Pop III/Pop II transition due to enrichment by outflows

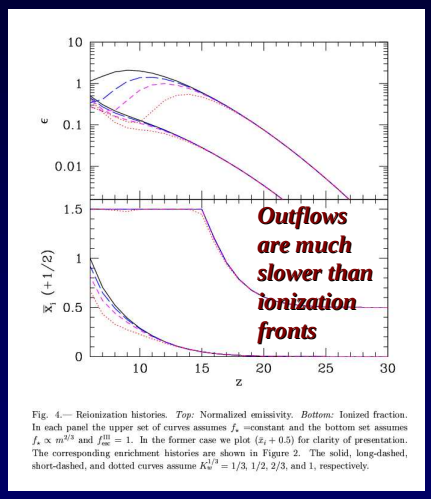

Fig. 4.— Reionization histories. *Top:* Normalized emissivity. *Bottom:* Ionized fraction. In each panel the upper set of curves assumes f_* =constant and the bottom set assumes $f_* \propto m^{2/3}$ and $f_{esc}^{III} = 1$. In the former case we plot $(\bar{x}_i + 0.5)$ for clarity of presentation. The corresponding enrichment histories are shown in Figure 2. The solid, long-dashed, short-dashed, and dotted curves assume $K_w^{1/3} = 1/3, 1/2, 2/3$, and 1, respectively.

Change in minimum galaxy mass due to photoionization heating/ H_2 *dissociation*

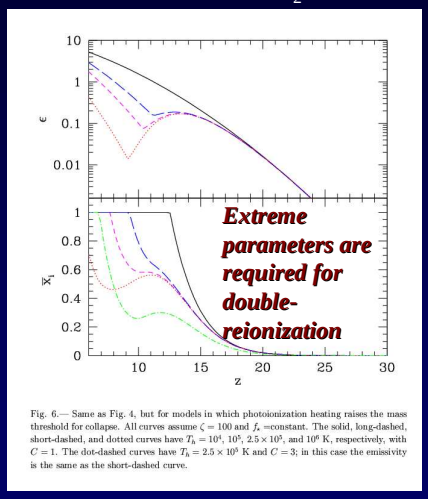

Fig. 6.— Same as Fig. 4, but for models in which photoionization heating raises the mass threshold for collapse. All curves assume $\zeta = 100$ and f_* =constant. The solid, long-dashed, short-dashed, and dotted curves have $T_h = 10^4$, 10^5, 2.5×10^5, and 10^6 K, respectively, with $C = 1$. The dot-dashed curves have $T_h = 2.5 \times 10^5$ K and $C = 3$; in this case the emissivity is the same as the short-dashed curve.

Probably not…but extended

Furlanetto & Loeb, astro-ph/0409656

Other Feedback from First Stars

Binding Energy of Dark Matter Halos

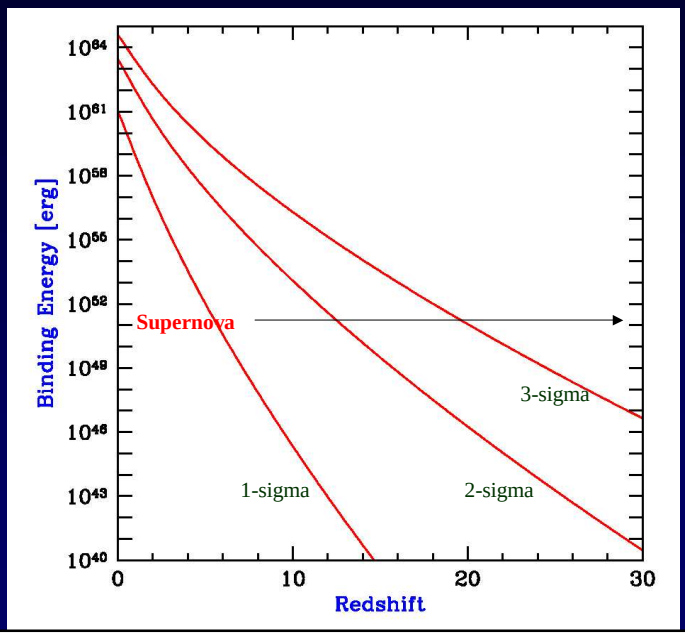

Self-Regulated Star Formation

Virial temperature < 10,000K

H_2 *destruction by starlight (10.2<E<13.6 eV)*

Evaporation of gas cloud by photo-ionization heating to >10,000K

Virial temperature > 10,000K

$$M_? / E_{SN} \propto \frac{3}{2} M_{gas} \hat{u}^2$$

(Dekel & Silk 1986)

$$f_? = \frac{M_?}{M_{gas}} / \hat{u}^2 / M_{halo}^{2=3}$$

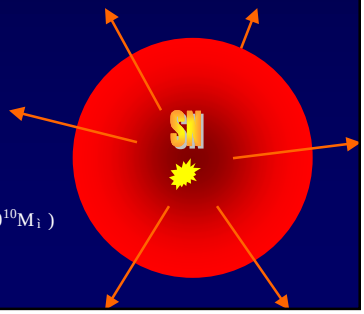

As observed for local dwarf galaxies ($M_? < 3 \times 10^{10} M_\odot$)

in SDSS (Kaufmann et al. 2002)

Gamma-Ray Bursts: Probing one Star at a Time

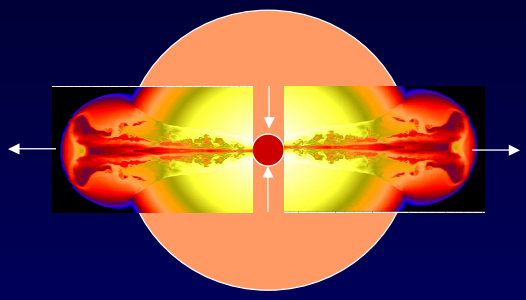

Collapse of a Massive Star

(accompanied by a supernova)

Detectability of Afterglow Emission Near the Lya Wavelength

Photometric redshift identification: based on the Lya trough

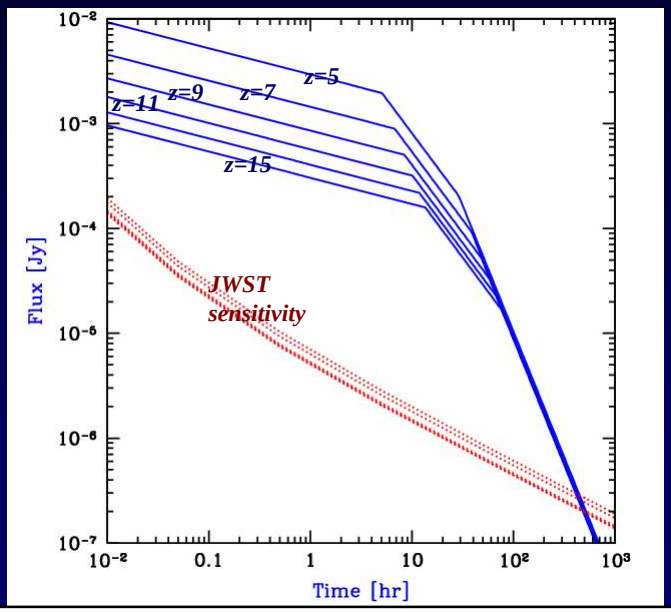

Barkana & Loeb 2003

astro-ph/0305470

Gamma-Ray Burst Afterglows

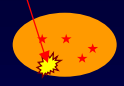

$M_{ionized} \propto 4 \times 10^4 M_\odot \times \frac{E}{10^{51} ergs}$

Weak contamination by Lya emission line

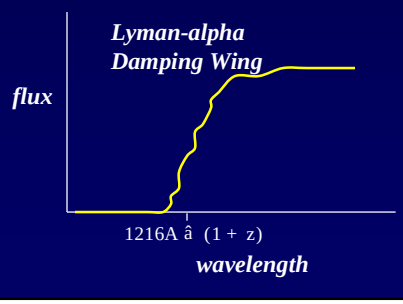

Quasars

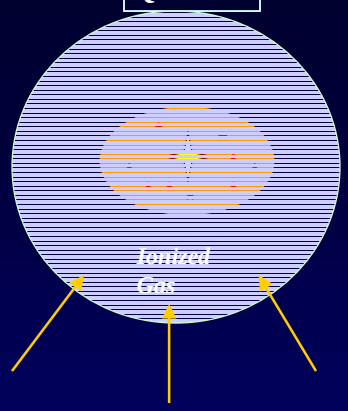

Infall onto Massive Host Galaxy

Quasars get fainter with increasing redshift because galaxies are less massive and the luminosity distance increases at higher redshifts!

Advantages of GRB Afterglows Relative to Quasars
(see details in astro-ph/0307231)

- *Luminous stellar sources) high redshifts*
  - outshine galaxies and quasars, as they become less luminous at increasingly higher redshifts
  - -ray trigger allows all-sky monitoring
- *Featureless broad-band spectra extending into the rest-frame UV*
  - absorption features can be used to probe the ionization and metallicity states of the IGM
- *Observed flux at a fixed observed age does not fade significantly with increasing GRB redshift* (cosmological time stretching counteracts increase in luminosity distance)
- *Weak Feedback on Surrounding IGM*
  - *Short-lived event:* negligible ionizing effect of a GRB on the IGM
  - *Low mass host galaxies:* weak IGM infall & *Lya* line emission

Fraction of GRBs Above a Given Redshift

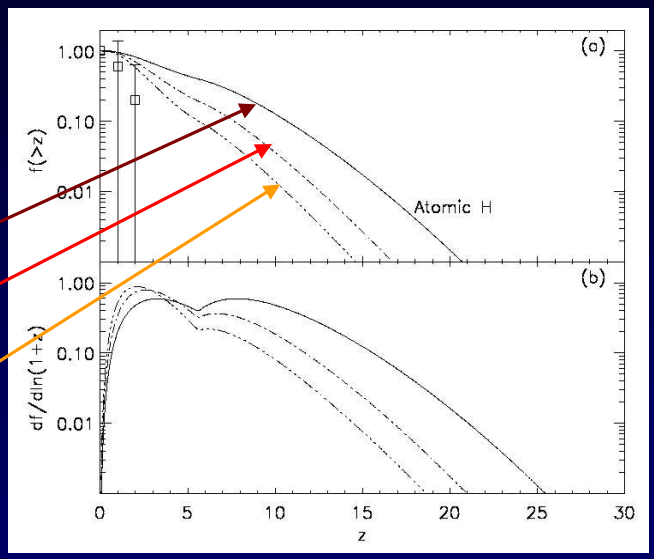

All GRBs

Swift

BATSE

Bromm & Loeb 2002

Results are sensitive to the uncertain GRB luminosity function.

Probes of Neutral Hydrogen: 21 cm Absorption

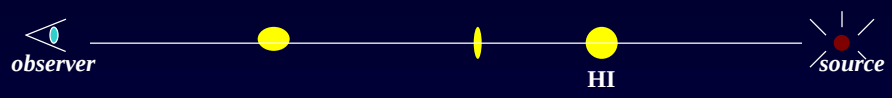

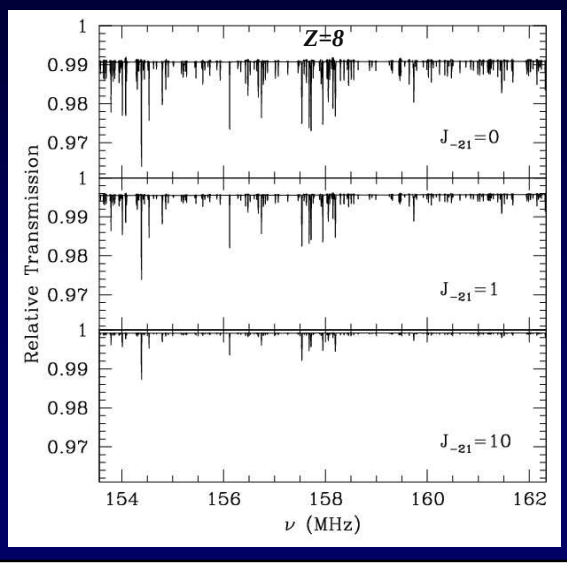

Contributions:

**Gaseous mini-halos and disks*

(Furlanetto & Loeb 2002)

**Sheets and filaments in the intergalactic medium*

(Carilli, Gnedin, & Owen 2002)

Detection with the planned Low Frequency Array (LOFAR) and Square Kilometre Array (SKA) is feasible for sources brighter than 10 mJy at z~10.

How Did the First Massive Black Holes Form?

Formation of Massive Black Holes in the First Galaxies

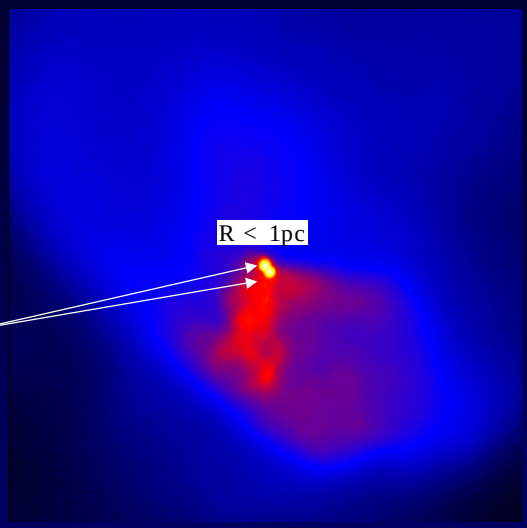

M_1 ø 2:2 â $10^6 M_ì$
M_2 ø 3:1 â $10^6 M_ì$

õ = 0:05

H_2 suppressed

Low-spin systems: Eisenstein & Loeb 1995

Numerical simulations: Bromm & Loeb 2002

Supermassive Stars

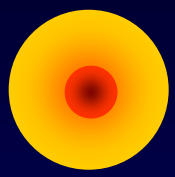

T_{eff} ø 10^5K

$L = L_E / M$

For a spherical (non-rotating) star: general-relativistic instability at

$$\left(\frac{GM}{Rc^2}\right)_{crit} = 0{:}6295\left(\frac{M_ì}{M}\right)^{1=2}$$

Angular momentum → mass shedding along equator

Collapse to a black hole is inevitable for $M > 300 M_ì$

$(N_{Quasars}=N_{Galaxies}) < 10^{à\ 2}$; $(M_{bh}=M_{galaxy}) < 10^{à\ 3}$

Why Are Quasars Short Lived?

Because they are suicidal!

<u>Principle of Self Regulation:</u> *supermassive black holes grow until they release sufficient energy to unbind the gas that feeds them from their host galaxy*

→*Implies a correlation between black hole mass and the depth of the gravitational potential well of its host galaxy*

Self-regulation of Supermassive Black Hole Growth

$L t_{dyn}$ ø $\frac{3}{2} M_{gas} \hat{u}^2$

dynamical time of galactic disk

halo velocity dispersion

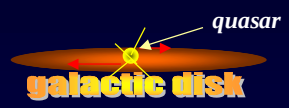

$\max f L g = L_E / M_{bh}$

$$! \quad \frac{M_{bh}}{10^8 M_{\grave{\imath}}} = 1{:}5 \quad \frac{\hat{u}}{200 km=s}^{5}$$

After translating ! ? *this relation matches the observed* M û ã *correlation in nearby galaxies (Tremaine et al. 2002; Ferarrese & Merritt 2002)*

Silk &Rees 1998; Wyithe & Loeb 2003

Correlation between black hole mass and velocity dispersion of host stellar system

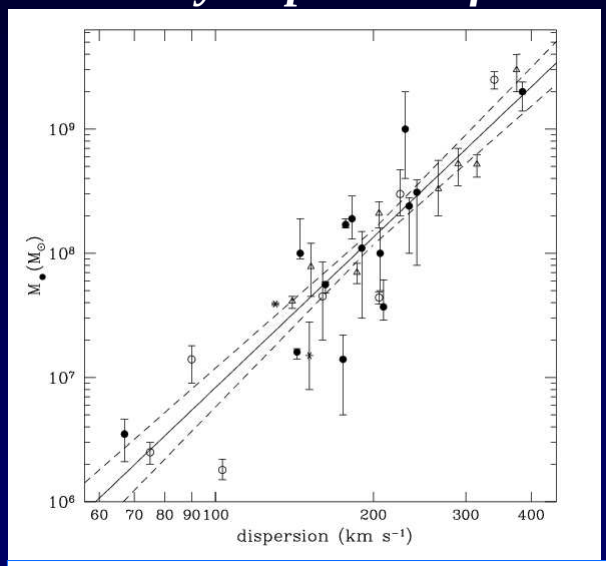

ì = 4:02 æ 0:32

ë = 8:13 æ 0:06

Tremaine et al. 2002

ì = 4:58 æ 0:52

= 8:22 0:07

Ferrarese 2002

log(M=M¡) = ë + ì log(û?=200km=s)

Quasar Luminosity Function

Simple physical model:

****Each galaxy merger leads to a bright quasar phase during which the black hole grows to a mass*** $M_{\bullet} / v_c^5$ ***and shines at the Eddington limit. The duration of this bright phase is dictated by the dynamical time of the host galactic disk (7% of the total energy release can unbind the disk on its dynamical time).***

****Merger rate: based on the extended Press-Schechter model in a LCDM cosmology.***

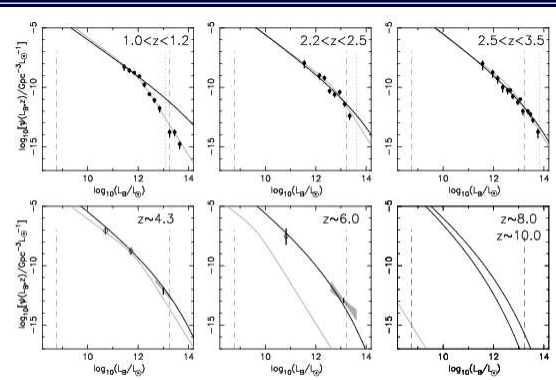

FIG. 1.— Comparison of the observed and model luminosity functions. The data points at $z \lesssim 4$ are summarized in Pei (1995), while the light lines show the double power-law fit to the 2dF quasar luminosity function (Boyle et al. 2000). At $z \sim 4.3$ and $z \sim 6.0$ the data is from Fan et al. (2001a;2001b;2003). The grey regions show the 1-σ range of logarithmic slope ([−2.25, −3.75] at $z \sim 4.3$ and [−1.6, −3.1] at $z \sim 6$), and the vertical bars show the uncertainty in the normalization. The open circles show data points converted from the X-ray luminosity function (Barger et al. 2003) of low luminosity quasars using the median quasar spectral energy distribution. In each panel the vertical dashed lines correspond to the Eddington luminosities of BHs bracketing the observed range of the M_{bh}-v_c relation, and the vertical dotted line corresponds to a BH in a $10^{13.5} M_\odot$ galaxy.

duty cycle ~10 Myr

Wyithe & Loeb
astro-ph/0304156

Clustering Statistics of Quasars

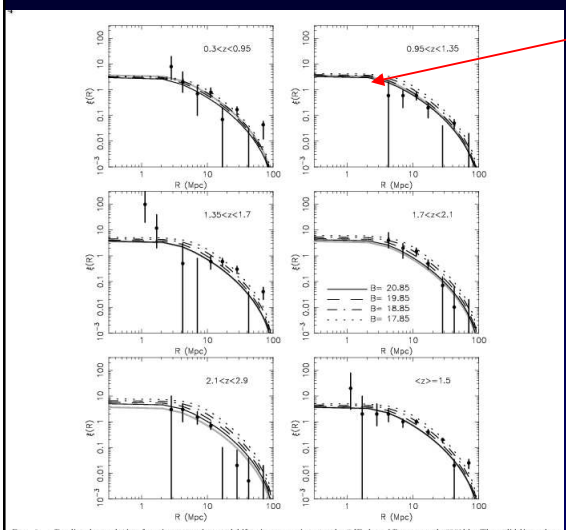

FIG. 1.— Predicted correlation function at various redshifts, in comparison to the 2dF data (Croom et al. 2001b). The solid lines show the correlation function predictions for quasars of various apparent B-band magnitudes (B). The 2dF limit is $B \sim 20.85$. The lower right panel shows data from entire 2dF sample in comparison to the theoretical prediction at the mean quasar redshift of $\langle z \rangle = 1.5$. The $B = 21$ prediction at this redshift is also shown by thick gray lines in the other panels to guide the eye. This case assumes $M_{bh} \propto v_c^5$, normalized to local observations, and $\eta = 1$ (case **A1**).

Lines: *correlation function of model with*

$$M_{bh} / v_c^5$$

$$L = L_E \quad \textit{(SIS)}$$

Data points:

2dF Quasar Survey (Boyle et al. 2000)

Wyithe & Loeb 2004; astro-ph/0403714

Data on Quasar Clustering/LF Implies:

- Local relation between galactic halo/black-hole + redshift evolution of quasar correlation length are consistent with M_{bh} / v_c^5
  and not $M_{bh} / M_{halo}^{5=3}$
- If mergers trigger quasar activity, then quasar lifetime scales with dynamical time of host galaxy / $(1 + z)^{\text{à } 3=2}$ rather than the redshift-independent Salpeter-Eddington time for its growth

  $t_E = 4 \text{ â } 10^7 (\text{ï}=0:1) \text{years}$

Wyithe & Loeb 2004; astro-ph/0403714

Hydrodynamic Simulations of Quasar Feedback

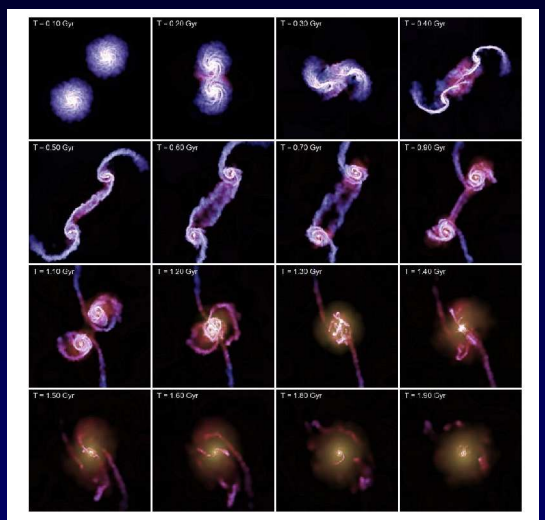

Figure 11. Evolution of the gas distribution in a major merger of two disk galaxies. Colour hue encodes gas temperature, while brightness indicates gas density. Each frame measures $50\,h^{-1}$ kpc on a side, and the corresponding time of each image is given by the labels. In this simulation, a slightly softer EOS ($q_{\rm EOS} = 0.25$) than in our default multiphase model was used.

(Springel, Di Matteo, & Hernquist 2004)

M = min{Bondi à rate; Eddington à rate}
energy à feeding à rate = 5% â 10% â Mc^2

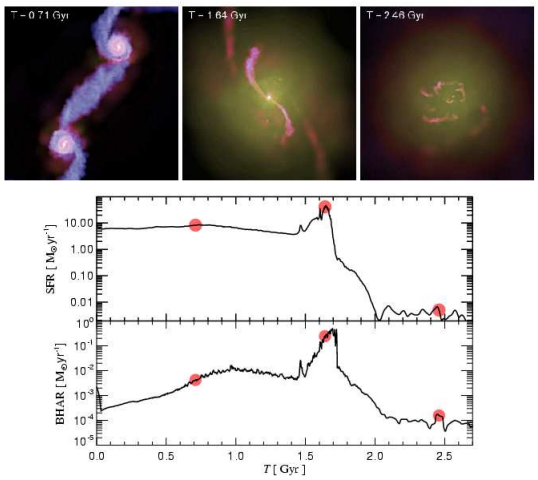

Figure 14. Merger of two disk galaxies, including the effects of black hole growth and AGN feedback. The images show the gas distribution in the two disks at three different times, where colour hue encodes temperature while brightness measures gas density. The bottom panels show the time evolution of the accretion rate onto the black holes (top) and the star formation rate (bottom). The red symbols in these panels mark the three times shown in the images on top. The first snapshot shows the system just after the first passage of the two disks. The second snapshot captures the system when the galaxies are coalescing, at which point the star formation and accretion rates peak. Finally, the third snapshot shows the system after the galaxies have fully merged, and most of the mass has settled into a slowly evolving remnant.

(Springel, Di Matteo, & Hernquist 2004)

*New Insights About Reionization**

- *Intergalactic hydrogen was significantly neutral at z~6.3.*
- *Low-mass stars started to form at a carbon/oxygen abundance of ~0.1% solar.*
- *Current numerical simulations of reionization are significantly biased due to their periodic boundary conditions.*
- *GRBs are ideal probes of reionization.*
- *21cm absorption map of CMB from z=30-200 provides the largest data set on the sky.*

Collaborators: *Rennan Barkana, Volker Bromm, Staurt Wyithe*

**All insights are described in papers posted on astro-ph over the past 12 months.*

Predicted Redshift Distribution of GRBs

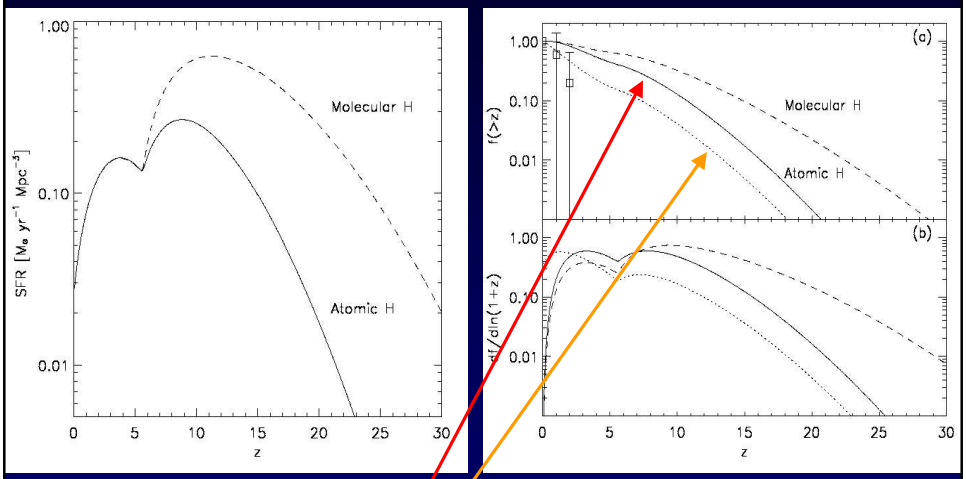

GRB fraction with redshift >z on the sky

Fraction of stellar mass formed by redshift z

Bromm & Loeb 2002

Swift Overview

Catching Gamma Ray Bursts on the Fly

Capabilities

- ~ 1000 GRBs studied over a three-year period
- 0.3–2.5 arc-second positions for each GRB
- Multiwavelength observatory (gamma, X-ray, UV, and Optical) to monitor afterglows
- 20–70 s reaction time
- Five times more sensitive than BATSE
- Spectroscopy from 0.2 to 150 keV
- Six colors covering 170–650 nm
- UV and optical spectroscopy with R ~ 300–600 for $M_b < 17$
- Capability to directly measure redshift
- Results publicly distributed with seconds

Planned for launch in 2004

Challenge: select photometrically all high-redshift GRBs (using the Lya break) and follow-up on them spectroscopically